ANALYSIS OF THE IMPACTS OF WAVE ENERGY CONVERTER ARRAYS ON THE NEARSHORE WAVE CLIMATE

Annika M. O'Dea[1]
Coastal & Ocean Engineering Program
School of Civil & Construction Engineering
Oregon State University
Corvallis, OR, USA

Merrick C. Haller
Coastal & Ocean Engineering Program
School of Civil & Construction Engineering
Oregon State University
Corvallis, OR, USA

[1]Corresponding author: odeaa@onid.oregonstate.edu

ABSTRACT

This study analyzes the impacts of offshore Wave Energy Converter (WEC) arrays on far-field waves and on nearshore wave-induced hydrodynamic forcing for a variety of array designs and incident wave conditions. The main objective of the study is to provide general conclusions on the nearshore impacts of WEC arrays in order to facilitate the assessment of future field test sites. The study utilizes the spectral wave model SWAN. Two array configurations are simulated, and WEC arrays are located either 5, 10, or 15 km offshore. Input conditions include parametric JONSWAP spectra with a range of offshore wave heights and periods. Trials are conducted with a directional wave field with the dominant direction being shore normal in all cases. Arrays are represented in SWAN through the external modification of the wave spectra at the device locations based on an experimentally-determined Power Transfer Function. Based on an analysis of existing field data, a new threshold for nearshore hydrodynamic impact is also established. The threshold represents an empirical relationship between radiation stress and longshore current magnitude. This threshold value is subsequently used as an indicator of when significant changes in the nearshore forcing are induced by WEC arrays. Results show that the changes in nearshore forcing parameters decrease as the distance between the array and the shore increases. Additionally, a more significant change in nearshore forcing parameters is seen in cases with larger input wave heights and periods and with low directional spread. The incident wave conditions, array configurations, and array locations that lead to nearshore impact are identified and assessed.

INTRODUCTION

Commercial exploitation of wave energy will require the deployment of arrays of Wave Energy Converters (WECs) that include several to hundreds of individual devices. Before WEC arrays can be deployed, efforts must be made to understand the potential impacts of WEC arrays on the incident wave climate.

Waves interact with WEC devices in ways that both alter device performance in the array (near-field effects) and modify the wave climate at some distance behind the array (far-field effects). The far-field effects of WEC arrays include a redirection of waves and a reduction in wave height in the lee of the array, referred to as the wave shadow. The extent of the far-field effects depends on the design of the array, its location, and the incident wave conditions. Quantifying the effect of WEC arrays on nearshore forcing and determining whether these changes could influence nearshore processes is crucial in limiting the potential environmental impacts of marine energy extraction.

A number of previous studies on WEC arrays have been conducted using spectral models such as SWAN to simulate the effects on the wave field [1-4]. Many past studies have represented the array as single or multiple partially transmissible objects with a frequency-independent transmission coefficient [1-3]. This technique fails to capture the frequency-dependent energy extraction characteristics that are inherent to WEC devices. The amount of energy that real devices extract is dependent on the device's Power Transfer Function (PTF), defined as the proportion of available wave power extracted at each frequency by a particular device. Smith et al [4] used a frequency-dependent extraction technique with a hypothetical PTF to assess the far-field effects of WEC arrays at the Wave Hub

site in the UK. In the present study, the representation of WEC devices in SWAN is further improved through the use of an experimentally-determined PTF established in an earlier laboratory study using scaled point absorber type WEC devices [5].

Although a few recent studies on WEC arrays have coupled nearshore wave models with current or sediment transport models [2, 6-7], most studies on nearshore impacts focus primarily on the differences in wave height and direction in the lee of the array [1, 3, 4, 8]. Nearshore wave height and direction are directly related to the wave radiation stresses that drive longshore currents, rip currents, and nearshore sediment transport. Although changes in wave height and direction therefore imply a change in nearshore forcing, the forcing terms in the nearshore hydrodynamic balance can be more directly quantified through an analysis of the radiation stress gradients [9]. This study aims to assess nearshore impacts through a direct analysis of these nearshore force parameters.

The impacts of WEC arrays will ultimately depend on the characteristics of the array (number of devices, spacing between devices, distance from shore) and the characteristics of the site (local wave climate, bathymetry). However, the use of generalized descriptions of the impacts of WEC arrays as basic guidelines in the design process would allow for a more rapid assessment of candidate sites. The main goal of this study is to analyze the nearshore impacts of WEC arrays on a generic nearshore configuration in order to draw general conclusions that could be used to facilitate the preliminary design and development of future arrays.

This study can be broken into three parts. The goal of the first part is to develop a methodology for assessing the impacts of WEC arrays on nearshore forcing parameters using a realistic representation of WEC energy extraction in SWAN. The goal of the second part is to determine a representative threshold longshore force F_y level based on existing radiation stress and current field data. The goal of the final part is to determine how array spacing and distance from shore influence nearshore forcing, and to determine which array designs and incident wave conditions generate longshore forces that exceed this threshold. In order to determine whether the general conclusions made in this idealized study can be applied to field sites with more complicated bathymetries, this same methodology is being applied to two WEC test sites off the coast of Newport, OR, and the results will be compared to the conclusions drawn in the current study.

METHODS
Numerical Model
Overview of SWAN

Simulating WAves Nearshore (SWAN) is a third-generation spectral wave model specifically developed to model nearshore wave transformation. SWAN uses the spectral action balance equation to calculate the evolution of wave spectra. The spectral action balance is shown in Equation 1,

$$\frac{\partial N}{\partial t} + \frac{\partial c_x N}{\partial x} + \frac{\partial c_y N}{\partial y} + \frac{\partial c_\sigma N}{\partial \sigma} + \frac{\partial c_\theta N}{\partial \theta} = S_{tot} \qquad (1)$$

where N is the energy density, c_x and c_y are the velocity components of N in geographical space, θ is the wave direction, σ is the relative frequency, and c_σ and c_θ are the propagation velocities of N in σ- and θ-space. The term S_{tot} represents the sum of the physical processes that result in the generation, redistribution, and dissipation of energy. These processes include wave growth through energy transfer from wind (energy generation), nonlinear transfer of wave energy through quadruplet and triad interactions (energy redistribution), as well as the loss of energy through wave breaking, bottom friction, and white-capping (energy dissipation). In this study, only depth-induced breaking was included from this list of physical processes.
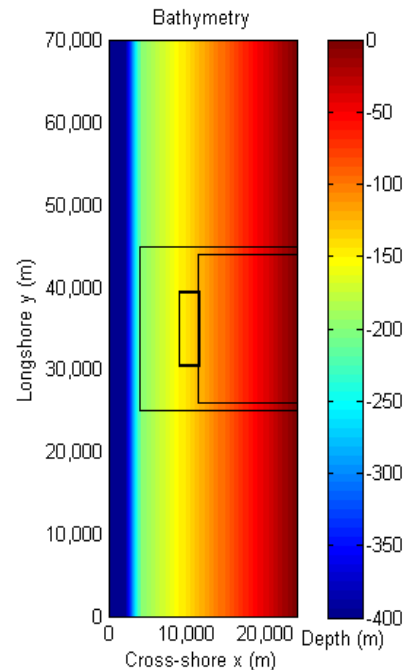
Model Domain

FIGURE 1. MODEL BATHYMETRY FOR CASES WITH AN ARRAY 15 KM FROM SHORE. BLACK LINES INDICATE A NESTED GRID WITH A DIFFERENT SPATIAL RESOLUTION.

For the parametric study on the nearshore impacts of WEC arrays we used a 24 km by 70 km model domain discretized into a regular grid with a spatial resolution of 200 m. Within this domain, four smaller, higher resolution grids were nested (Figure 1). The bathymetry consisted of an offshore section with a cross-shore length of 2 km and a constant depth of 400 meters, followed by a 2 km section with a 1:10 slope, and finally a 20 km planar shelf with a slope of 1:100. The spatial resolution increased from 200 m in the largest grid to 50 m in the 20 km by 20 km nested grid. A spatial resolution of 9 m was used in the vicinity of the WEC array, followed by a spatial resolution of 18m in the nearshore zone. In order to resolve the effects of the individual WECs on the wave field, the wave action density spectra were discretized into 720 directional bins and 40 frequency bins. WEC arrays were located either 5, 10, or 15 km offshore.

Input Conditions

JONSWAP spectra were used as input conditions at the offshore boundary. Trials were conducted with two input significant wave heights (2 and 6 m), nine input peak periods (6, 7, 8, 9, 10, 12, 14, 16, and 18 s), and two directional spreads (14° low directional spread and 35° high directional spread). A total of 36 sets of wave conditions were simulated. Trials were conducted with these input conditions using both array configurations (closely-spaced and widely-spaced) and with arrays located at each distance from shore (5, 10, and 15 km). Simulations were also made without an array for each set of input conditions. A total of 252 trials were conducted.

Representation of WECS in SWAN

The PTF was determined in a previous laboratory study conducted in the Tsunami Wave Basin at the O.H. Hinsdale Wave Research Laboratory using scaled versions of Columbia Power Technologies' Manta Buoy, a point absorber type WEC [5]. The laboratory PTF was then scaled to have a peak period of extraction at 9 s, which is the average annual energy period on the Oregon coast [10]. The PTF as a function of wave frequency is shown in Figure 2.

The PTF represents the proportion of wave energy extracted across the diameter of a device as a function of frequency. Subtracting the PTF from 1 (at each frequency) therefore gives the proportion of wave energy remaining in the wave field after the device. Wave spectra were externally modified at the device locations using Equation 2,

$$S_{after} = S_{before} * (1 - PTF) \qquad (2)$$

where S_{before} is the spectral energy density in the wave field before the device, and S_{after} is the spectral energy density in the wave field after the device.

The measured PTF from the laboratory work exceeds one for a narrow range of frequencies. This is indicative of increased energy capture efficiency and is made possible through the process off wave diffraction. In order to capture this behavior in the model it would be necessary to artificially increase the device diameter. However, where the experimental PTF was greater than 1, we chose to cap the PTF at a value of 1.
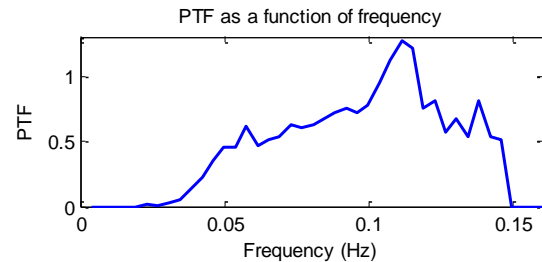

FIGURE 2. THE EXPERIMENTALLY DETERMINED PTF AS A FUNCTION OF FREQUENCY [5].

WEC arrays included 60 devices in two staggered rows (Figure 3). Each device had a diameter of 18 m. To assess the importance of spacing between devices, both closely-spaced and widely-spaced arrays were simulated for each set of input wave conditions. Closely-spaced arrays had a distance of 72 m (4 times the WEC diameter) between devices and rows, and widely-spaced arrays had a distance of 180 m (10 times the WEC diameter) between devices and rows.
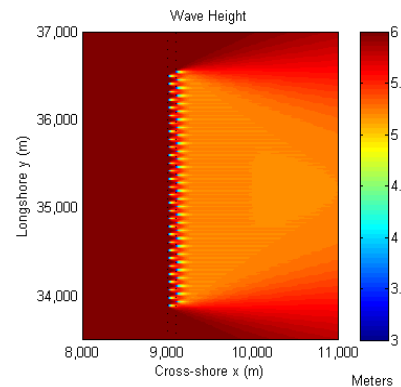

FIGURE 3. WEC ARRAY REPRESENTATION IN SWAN, SHOWN HERE IN A PLOT OF WAVE HEIGHT (H_S = 6 M, T_P = 12 S, LOW DIRECTIONAL SPREAD), WITH A 60-DEVICE, CLOSELY-SPACED ARRAY.

Model Outputs

For each trial, wave height H_s, wave direction θ, peak period T_p, and the wave-induced forces

3

were calculated at each grid point across the domain. The wave-induced forces in the cross-shore (F_x) and the longshore (F_y) direction are shown in Equations 3 and 4,

$$F_x = -\frac{dS_{xx}}{dx} - \frac{dS_{xy}}{dy} \qquad (3)$$

$$F_y = -\frac{dS_{yx}}{dx} - \frac{dS_{yy}}{dy} \qquad (4)$$

where S_{xx}, S_{xy}, S_{yx}, and S_{yy} are the radiation stress terms. The radiation stress terms are a function of both wave energy (and therefore the square of the wave height) as well as wave direction. These terms are shown in Equations 5, 6, and 7,

$$S_{xx} = E[n(\cos^2\theta + 1) - \frac{1}{2}] \qquad (5)$$

$$S_{yy} = E[n(\sin^2\theta + 1) - \frac{1}{2}] \qquad (6)$$

$$S_{xy} = S_{yx} = \frac{E}{2}\sin2\theta \qquad (7)$$

where E is the wave energy, θ is the wave direction, k is the wave number, and h is the water depth, and with n given by Equation 8 [9].

$$n = \frac{1}{2}\left(1 + \frac{2kh}{\sinh2kh}\right). \qquad (8)$$

Threshold Longshore Force Value

Guza et al. [11] and Feddersen et al. [12] have demonstrated that a strong correlation exists between S_{xy} at a fixed point outside the surf zone and the maximum longshore current velocity. Their data were collected during several large-scale field experiments conducted at the US Army Corps of Engineers Field Research Facility (Duck, NC). Feddersen et al. [12, see their Figure 4] showed an approximately linear relationship between S_{xy}/ρ measured at the 8 m depth contour and the maximum of the measured longshore current velocity profile. For our study we defined (somewhat arbitrarily) 20 cm/s as a threshold for significant longshore current magnitude, which according to the Feddersen et al. data translates to a threshold S_{xy}/ρ value of approximately 0.1 m³/s² (at the 8 m contour line).

However, we note that equations (3) and (4) show that the nearshore forcing terms are not directly dependent on the radiation stress magnitudes, but on their spatial gradients. Specifically, the cross-shore gradient of S_{xy} is the dominant forcing term in the total longshore forcing F_y. Hence, in order to relate the longshore current threshold to a threshold of the longshore forcing F_y, we ran a set of SWAN simulations over a generic planar beach. The simulations use a

range of significant wave heights (0.5 m to 6 meters) and dominant wave directions (0° to 45°). Figure 4 shows the resulting S_{xy}/ρ at the 8 m contour line (top) as well as the maximum F_y (bottom), both plotted as a function of rms wave height and direction. Both parameters show an increase in magnitude with either an increase in wave height or an increase in wave direction. The $S_{xy}/\rho = 0.1$ m³/s² contour line was plotted on both figures, shown in red. By finding the F_y contour that most closely matches the $S_{xy}/\rho = 0.1$ m³/s² contour line, we were able to map the significant S_{xy}/ρ value to a significant F_y value, which was found to be 0.5 N/m². This value was used as a F_y threshold, and all F_y values that exceeded this threshold were considered significant enough to impact nearshore processes.
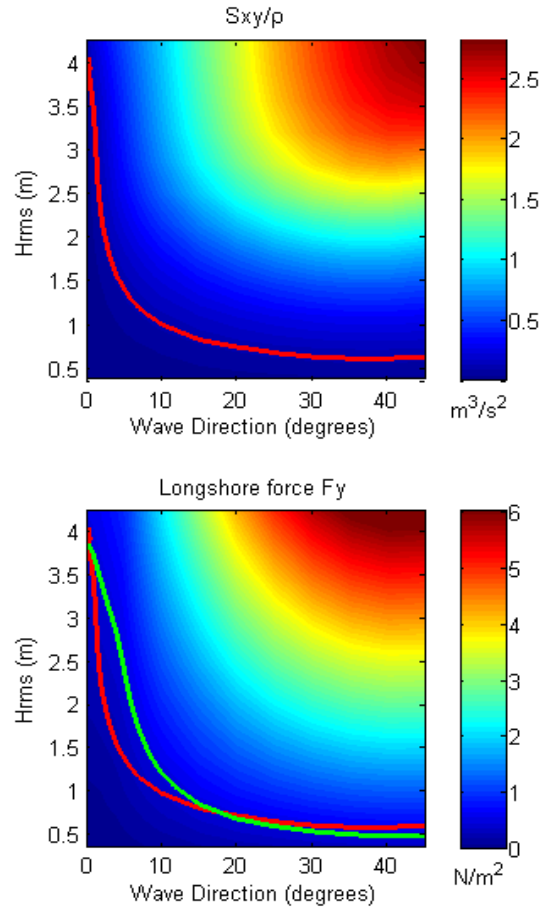

FIGURE 4. S_{XY}/ρ AT THE 8 M CONTOUR LINE (TOP) AND MAXIMUM F_Y (BOTTOM) AS A FUNCTION OF WAVE HEIGHT AND DIRECTION. THE $S_{XY}/\rho = 0.1$ M³/S² CONTOUR LINE IS SHOWN IN RED, ALONG WITH THE $F_Y = 0.5$ N/M² CONTOUR LINE IN GREEN.

RESULTS AND DISCUSSION
Parametric Study

Wave height H_s, wave direction θ, and wave-induced forces F_x and F_y were calculated at every grid point in the domain for each trial. Figure 5

TABLE 1. RESULTS FROM TRIALS WITH LOW DIRECTIONAL SPREAD INPUT CONDITIONS. TRIALS THAT GENERATED A LONGSHORE FORCE ABOVE THE THRESHOLD VALUE ARE MARKED WITH AN X.

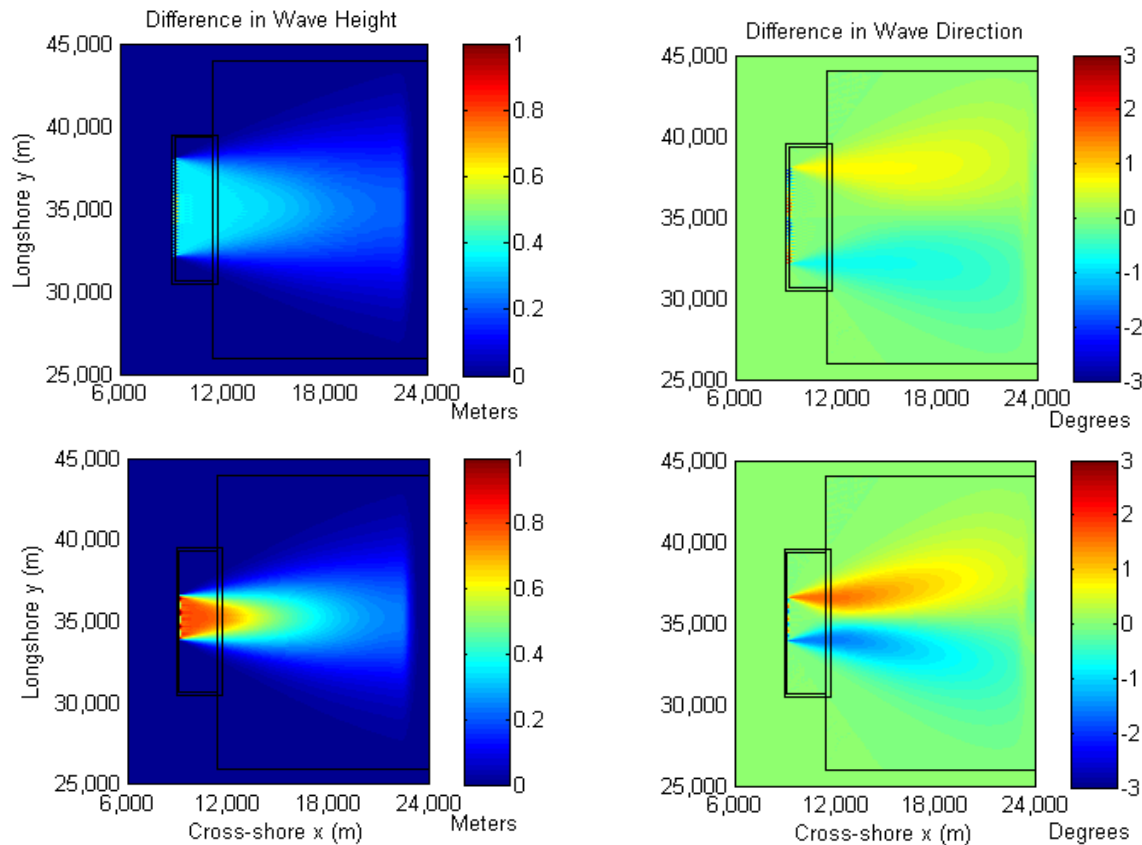|	5 km from shore										
	Hs (m)	Peak Period Tp (s)									
		6	7	8	9	10	12	14	16	18
4x spacing	6				X	x	x	x	x	x
	2									
10x spacing	6					x	x	x	x	x
	2									
	10 km from shore										
		6	7	8	9	10	12	14	16	18
4x spacing	6							x	x	x
	2									
10x spacing	6							x	x	x
	2									
	15 km from shore										
		6	7	8	9	10	12	14	16	18
4x spacing	6									
	2									
10x spacing	6								x	x
	2									

FIGURE 5. DIFFERENCES IN WAVE HEIGHT (LEFT) AND WAVE DIRECTION (RIGHT) FOR A WIDELY-SPACED ARRAY (TOP) AND A CLOSELY-SPACED ARRAY (BOTTOM) WITH AN INPUT WAVE HEIGHT OF 6 M, AN INPUT WAVE PERIOD OF 12 S, LOW DIRECTIONAL SPREAD, AND AN ARRAY LOCATED 15 KM FROM SHORE.
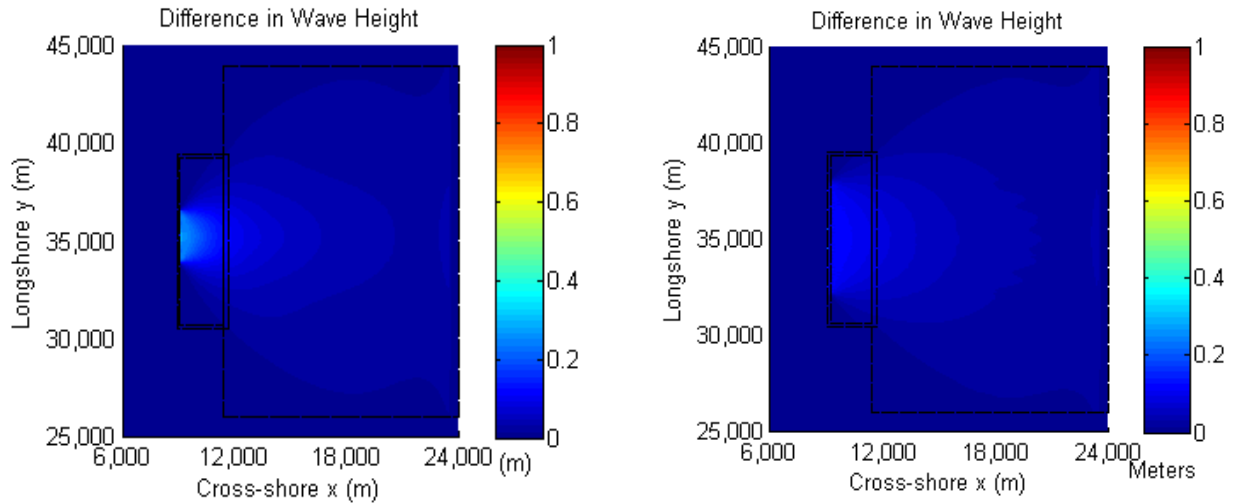
FIGURE 6. DIFFERENCES IN WAVE HEIGHT WITH A CLOSELY-SPACED ARRAY (LEFT) AND A WIDELY-SPACED ARRAY (RIGHT) WITH AN INPUT WAVE HEIGHT OF 6 M, AN INPUT WAVE PERIOD OF 12 S, HIGH DIRECTIONAL SPREAD, AND AN ARRAY LOCATED 15 KM FROM SHORE.

shows the differences in wave height and direction in the lee of both widely-spaced (top) and closely-spaced (bottom) WEC arrays for trials with an input wave height of 6 m, an input wave period of 12 s, low directional spread, and with an array located 15 km from shore. The reduction in wave height and the redirection of waves due to the WEC array is clearly visible. The diffraction of waves into the wave shadow results in a positive change in direction to one side of the array and a negative change in direction to the other side of the array (Figure 5). The direction of F_y depends on the incident wave angle as it approaches the shore. The spatial variability in the direction of the incident waves due to the WEC array therefore has significant implications for F_y.
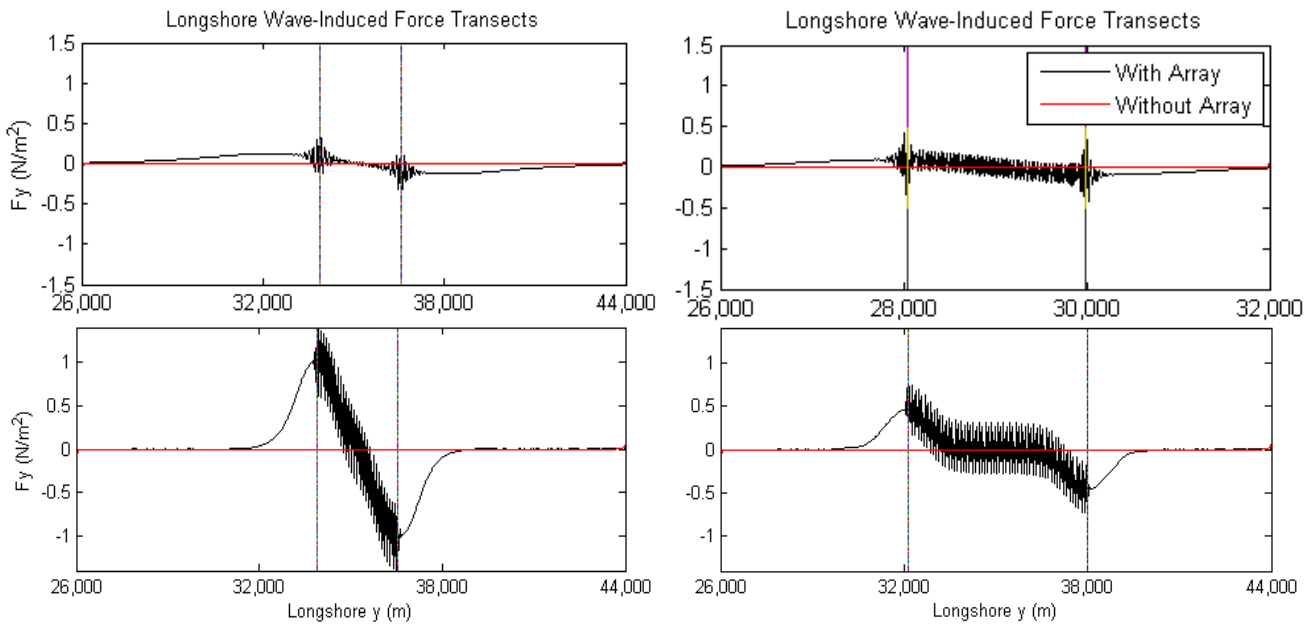

FIGURE 7. LONGSHORE TRANSECTS OF F_Y AT THE BREAKER LINE IN THE LEE OF A CLOSELY-SPACED ARRAY (LEFT) AND A WIDELY-SPACED ARRAY (RIGHT) WITH ARRAYS LOCATED 15 KM OFFSHORE (TOP) AND 5 KM OFFSHORE (BOTTOM) FROM TRIALS WITH AN INPUT WAVE HEIGHT OF 6 M, AN INPUT WAVE PERIOD OF 12 S, AND LOW DIRECTIONAL SPREAD. THE VERTICAL LINES SHOW THE LONGSHORE LOCATION OF THE WEC ARRAY.
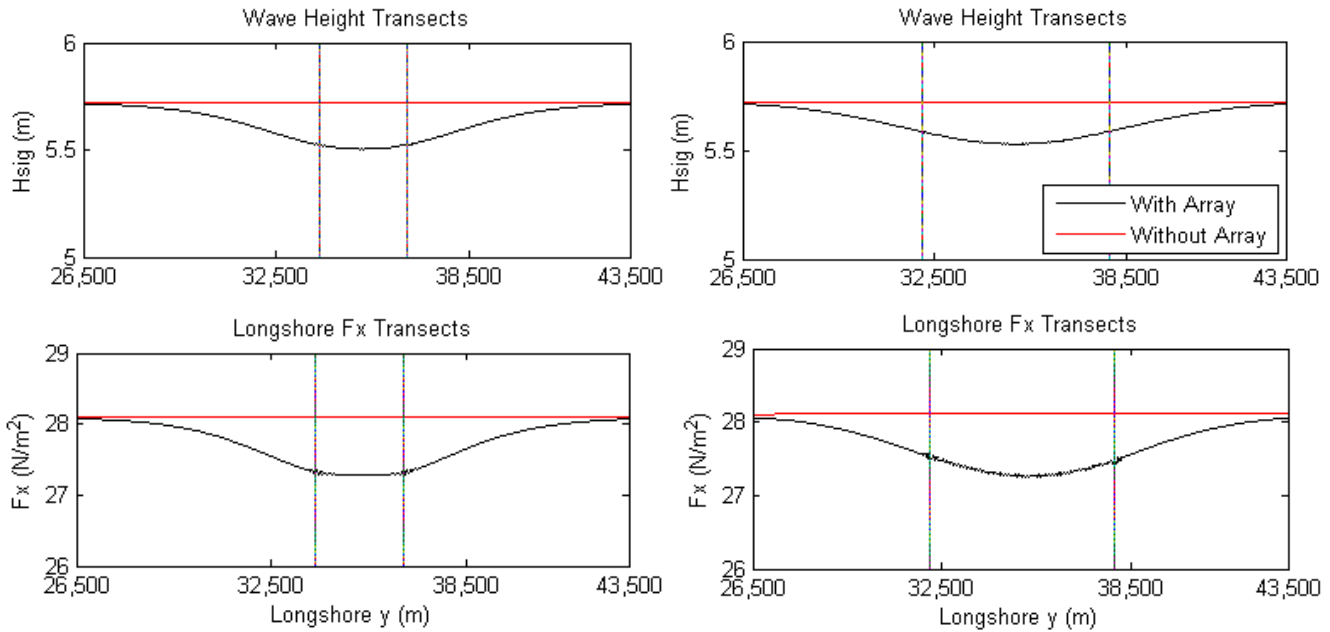
FIGURE 8. LONGSHORE TRANSECTS OF WAVE HEIGHT AT THE BREAKER LINE (TOP) AND THE MAXIMUM CROSS-SHORE FORCE (BOTTOM) FOR A CLOSELY-SPACED ARRAY (LEFT) AND A WIDELY-SPACED ARRAY (RIGHT) FROM TRIALS WITH AN INPUT WAVE HEIGHT OF 6 M, AN INPUT WAVE PERIOD OF 12 S, LOW DIRECTIONAL SPREAD, AND AN ARRAY LOCATED 15 KM FROM SHORE. THE VERTICAL LINES SHOW THE LONGSHORE LOCATION OF THE WEC ARRAY.

The maximum change in F_y at the breaking point was found for all trials. Generally, trials with larger input wave heights (6 m) and larger periods (>10 s) were more likely to reach the threshold F_y value. None of the trials with a 2 m input wave height or with a period under 9 s reached the threshold F_y value at the breaker line.

Both directional spread and the distance between the WEC and the shore were found to be important factors in the regeneration of waves in the lee of the array. A total of 19 cases with low directional spread (swell) were found to reach the threshold F_y value at the breaker line, summarized in Table 1. Only six cases with high directional spread (wind-seas) reached this same threshold. Three trials with high directional spread and with an array 5 km from shore reached the threshold F_y value (T_p = 14, 16, and 18s, H_s = 6 m, and a closely-spaced array) along with three trials with an array 10 km from shore (T_p = 14, 16, and 18 s, H_s = 6 m, and a widely-spaced array). Overall, high directional spread was found to increase wave regeneration in the lee of the array and therefore reduce the extent of the far-field effects. The increase in wave regeneration in trials with high versus low directional spread is visible in plots of the difference in wave height, shown in Figures 5 and 6 (with an input wave height of 6 m, an input wave period of 12 s, and with arrays located 15 km from shore).

The distance between the WEC array and the shore was also found to have a significant impact on the magnitude of the nearshore effects of the arrays. Less wave regeneration was possible in the lee of an array 5 km from shore, resulting in a more significant change in the magnitude of F_y at the breaker line for these cases. A total of 14 trials with the array located 5 km offshore reached the threshold F_y value (11 from cases with low directional spread, and 3 from cases with high directional spread). Only two trials with arrays located 15 km offshore reached this threshold (both with low directional spread).

WEC array spacing had an effect on both the magnitude and the extent of the far-field changes. Closely-spaced arrays resulted in a significantly larger change in wave parameters in the direct lee of the array (Figure 4), but the differences between cases based on WEC spacing decreased with increasing distance from the array. The magnitude of F_y at the breaker line was found to be larger in the lee of closely-spaced arrays when the array was 5 km from shore. Interestingly, the reverse was true for arrays 15 km from shore. In cases with arrays 15 km from shore, widely-spaced arrays were more likely to generate F_y values above the threshold at the breaker line.

To visualize the spatial differences in F_y across the domain, longshore F_y transects were plotted at the breaker line for trials with an input wave height of 6 m, an input wave period of 12 s, and

with low directional spread (Figure 7). The spatial difference in wave direction on either side of the array results in a similar spatial variability in the direction of F_y. The longshore force vector on either side of the array is directed toward the area directly behind the array, resulting in a convergence of force in this area.

Oscillating F_y values were seen at the breaker line in the direct lee of the array. Oscillating longshore forces can have significant impacts on nearshore processes and are especially important in the generation of rip currents [13]. The spacing and significance of these oscillations are a potential area of future study.

In addition to an increase in the magnitude of F_y, a decrease in the magnitude of F_x was seen in the lee of the array. Since the occurrence of depth-limited wave breaking leads to the largest radiation stress gradients, both F_x and F_y are strongest in the surf zone. Trends in F_x in the surf zone were found to be very similar to trends in H_s. Longshore transects of H_s at the breaker line and F_x at the location of its largest magnitude are shown in Figure 8 (with an input wave height of 6 m, an input wave period of 12 s, low directional spread, and with arrays located 15 km from shore). Maximum F_x values for cases with and without arrays were compared. A maximum reduction of 10% was seen in the magnitude of F_x with an array 5 km from shore, and a maximum reduction of 3% was seen in cases with an array located 15 km from shore. The maximum reduction in F_x was less than 8% for all trials for all trials with high directional spread.

Future Study

In order to assess the applicability of the conclusions made in this study to sites with more complicated bathymetries, the same methodology is being applied to two Northwest National Marine Renewable Energy (NNMREC) permitted test sites, the North Energy Test Site (NETS) and the South Energy Test Site (SETS), both located off the coast of Newport Oregon. The NETS site is shown in Figure 9. The domain bathymetry was created using the 1/3 arc-second Central Oregon Coast DEM from the National Geophysical Data Center (NGDC) [14]. Directional wave spectra from a WAVEWATCH III hindcast for 2011 are used as offshore inputs [15]. AWAC data from a 2011 field test at a site within the domain will be used for model validation [16]. The results from the current parametric study will be compared to the results from the analysis of the NETS and SETS sites to determine if the changes in nearshore forcing due to WEC arrays at the NETS and SETS follow the trends described in this paper.
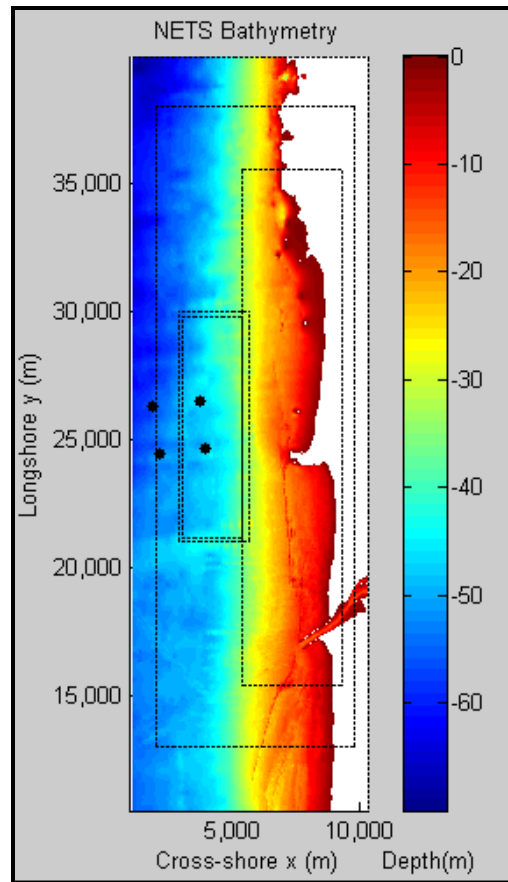

FIGURE 9. BATHYMETRY AT THE NETS TEST SITE (OUTLINED WITH FOUR BLACK DOTS). DOTTED LINES SHOW THE NESTED SWAN GRIDS.

CONCLUSIONS

A methodology for modeling WEC arrays in SWAN was developed and applied in this parametric study of the impacts of WEC arrays on nearshore forcing parameters. WEC arrays were incorporated in the SWAN domain through the external modification of the wave spectra at the devices locations. This technique employs an experimentally determined PTF that allows for a realistic representation of energy extraction by WEC devices. A threshold longshore force F_y value was defined to help assess the significance of the changes in nearshore forcing. Nearshore wave-induced forcing terms F_x and F_y were analyzed for each set of input conditions and for each WEC design.

Larger maximum F_y values at the breaking point were seen with larger input wave heights and larger input periods. Wave regeneration in the shadow zone was found to increase with an increase in the distance between the array and the shore and with an increase in directional spreading, implying that the largest differences in the nearshore forcing due to WEC arrays will occur in high energy swell seas with a WEC array

located close to shore. Closely-spaced arrays had a much larger impact on wave height and direction in the direct lee of the array, but the differences between cases due to WEC spacing decreased with increasing distance from the array. For arrays 5 km from shore, it was found that closely-spaced arrays had a larger impact on F_y at the breaker line. For arrays 15 km from shore, however, a larger impact was seen in the lee of widely-spaced arrays. The results from this study will be compared to the results of a similar study of two permitted NNMREC test sites to assess the validity of the conclusions made in this parametric study when applied to sites with more realistic bathymetries.

ACKNOWLEDGEMENTS

REFERENCES
[1] Millar, D.L.; Smith, H.C.M; and Reeve, D.E. 2007, "Modelling analysis of the sensitivity of shoreline change to a wave farm," Oc. Eng. 34, pp. 884-901.
[2] Rusu, E. and Soares, C.G. 2013, "Coastal impact induced by a Pelamis wave farm operating in the Portuguese nearshore," Renew. Energ. 58, pp. 34-49.
[3] Carballo, R. and Iglesias, G, 2013. "Wave farm impact based on realistic wave-WEC interactions," Energy 51, pp. 216-219.
[4] Smith, H.C.M.; Pearce, C.; and Millar, D.L, 2012. "Further analysis of change in nearshore wave climate due to an offshore wave farm: An enhanced case study for the Wave Hub site." Renew. Energ. 40, pp. 51-64.
[5] Rhinefrank, K., M. Haller, T. Ozkan-Haller, A. Porter, C. McNatt, P. Lenee-Bluhm, and Schumacher, E. 2013, Benchmark Modeling of the Near-Field and Far-Field Wave Effects of Wave Energy Arrays, Columbia Power Technologies Final Report, DE-EE0002658, U.S. Dept. of Energy, www.osti.gov/servlets/purl/1060889/.
[6] Gonzalez-Santamaria, R.; Zou, Q.P.; and Pan, S. 2013, "Impacts of a wave farm on waves, currents and coastal morphology in South West England," Estuar. Coasts 1, pp. 1-14.
[7] Mendoza, E.; Silva, R.; Zanuttigh, B.; Angelilli, E.; Andersen, T.L.; Marinelli, L.; Norgaard, J.Q.H.; and Ruol, P. 2013, "Beach response to wave energy converter farms acting as coastal defence." Coast. Eng., in press.
[8] Palha, A.; Mendes, L.; Fortes, C.J.; Brito-Melo, A.; and Sarmento, A. 2010, "The impact of wave energy farms in the shoreline wave climate: Portuguese pilot zone case study using Pelamis energy wave devices." Renew. Energ. 35, pp. 62-77.
[9] Svendsen, I.A, 2006, Introduction to Nearshore Hydrodynamics, World Scientific Publishing Co. Pte. Ltd., Singapore, Chap. 11,12.
[10] Lenee-Bluhm, P.; Paasch, R.; and Ozkan-Haller, H.T. 2011. "Characterizing the wave energy resource of the US Pacific Northwest." Renew. Energ. 36, pp. 2106-2119.
[11] Guza, R.T.; Thorton, E.B.; and Christensen Jr, N. 1986, "Observations of Steady Longshore Currents in the Surf Zone." J. Phys. Oceanogr. 16, pp. 1959-1969.
[12] Feddersen, F; and Guza, R.T. 1998, "Alongshore momentum balances in the nearshore," J. Geophys. Res. 103 (C8), pp. 15667-15676.
[13] Bowen, A.J. 1969, "Rip Currents 1. Theoretical Investigations." J. Geophys. Res. 74 (23), pp. 5467-5478.
[14] Carignan, K.S., L.A. Taylor, B.W. Eakins, R.R. Warnken, E. Lim, and Medley, P.R. 2009, "Digital Elevation Model of Central Oregon Coast: Procedures, Data Sources and Analysis," NOAA Technical Memorandum NESDIS NGDC-25, U.S. Dept. of Commerce, Boulder, CO, 38 pp.
[15] Garcia-Medina, G.; Ozkan-Haller, H.T.; Ruggiero, P.; and Oskamp, J. 2013, "An inner-shelf wave forecasting system for the US Pacific Northwest," Weather Forecast. 28, pp. 681-703.
[16] Vardaro, M.; Risien, C.; Wingard, C.; and Fram, J. 2011, In-Shore Mooring Test 2 (ISMT2) Science Data Report, Oregon State University, Coastal and Global Scale Nodes, Ocean Observatories Initiative.